OPEN ACCESS
International Journal of Innovations in Science & Technology
IJIST
P ISSN : 2618-1630
E ISSN : 2909-6130

Arsenic (v) Adsorption by Using Synthesized Iron Oxide Nanoparticles (Fe_2O_3-NPs) and Aluminum Oxide Nanoparticles (Al_2O_3-NPs)

Muhammad Tahir Turi[1], Ma Wei[1], Ittehad Hussain[2], Javid Hussain[3]
[1]Department of Chemistry & Chemical Engineering, Dalian University of Technology, Dalian 116023, PR China.
[2]Key Laboratory of Drinking Water Science and Technology, Research Center for Eco-Environmental Sciences, University of Chinese Academy of Sciences, Chinese Academy of Sciences, 18 Shuang-qing Road, Beijing 100085, China.
[3]Department of Environmental Science, Balochistan University of Information Technology, Engineering and Management Sciences, Quetta, 87300, Pakistan.
*__Correspondence:__ Muhammad Tahir Turi, __Email ID:__ engr.tahirturi@gmail.com
Citation | Turi.M.T, Wei.M, Hussain.I, Hussain.J "Arsenic (v) Adsorption by Using Synthesized Iron Oxide Nanoparticles (Fe_2O_3-NPs) and Aluminum Oxide Nanoparticles (Al_2O_3-NPs)," Int. J. Innov. Sci. Technol., vol. 4, no. 4, pp.1023-1041, 2022.
DOI | https://doi.org/10.33411/IJIST/2022040408
Received | Aug 25, 2022. **Revised** | Oct 20, 2022. **Accepted** | Oct 25, 2022. **Published** | Oct 30,2022.

Arsenic, is one of the most harmful elements to human health that continuously causes a threat to the world. Arsenic is found in combined form in rocks under the earth's surface and when it dissolves, it contaminates groundwater. The current research synthesized iron oxide nanoparticles (Fe_2O_3-NPs) and aluminum oxide nanoparticles (Al_2O_3-NPs) for removal of arsenic (As) (V) from an aqueous medium and characterized the synthesized material by different analytical techniques such as FT-IR spectroscopy and XRD spectroscopy. The results show successful synthesis of Fe_2O_3-NPs and Al_2O_3-NPs. Furthermore, the synthesized material was used as an adsorbent for extraction of as (V) from water. The effect of different parameters such as pH, temperature, contact time, and adsorbent dose on the adsorption process was investigated. The adsorption efficiency was determined by Fe_2O_3-NPs at about 20 mg/g and Al_2O_3-NPs at 19.5 mg/g. The quantitative removal of as (V) from industrial water required a minimum amount (0.2 g) of Fe_2O_3-NPs and Al_2O_3-NPs. various kinetic and isotherms were investigated in the current study. The result showed that the obtained data for Fe_2O_3-NPs was more fitted to Pseudo second order kinetic and Freundlich equation, while for Al_2O_3-NPs the data was more fitted to Pseudo second order kinetic and Elovich model equation, which confirms the interaction among as (V) and adsorbents. Thermodynamic parameters were also investigated which shows the process is spontaneous and endothermic. This model was used to estimate the site energy distribution for each adsorbent. Thermodynamic parameters were also investigated which shows the non-spontaneous and endothermic nature of the adsorbent. According to the results of the analysis of the approximate site energy distribution, adding Fe_2O_3 and Al_2O_3-NPs to arsenic decreased the area under the frequency distribution curve of the sorption site energies, which in turn decreased the number of sorption sites that were open to arsenic. This might be explained by the hydrophobic interaction between synthesized materials and arsenic being reduced due to the blocking of the Fe_2O_3 and Al_2O_3-NPs hydrophobic surface.

Keywords: Arsenic, Iron Oxide, Aluminum Oxide, Adsorption of Arsenic, Adsorbents

Acknowledgment.
I would like to express my sincere gratitude to my research supervisor, Dr. Ma Wei, Department of Chemistry & Chemical Engineering, Dalian University of Technology, China for their continuous support. Study-related research for their patience, motivation, and immense knowledge. I am also very thankful to all my seniors and fellows for their sincere support and fruitful discussion. Last but not the least, I would like to thank my family, my parents, and my siblings for supporting me & those who indirectly contributed to this research, your kindness means a lot to me

Author's Contribution.
Each Author has made a complete contribution regarding this research.

Conflict of interest:
We have no conflicts of interest to disclose, all authors have read the final manuscript and have approved the submission to the journal, and have accepted full responsibility for the manuscript's delivery and contents. There exists no conflict of interest for publishing this manuscript in IJIST.

Project details. Nil

Introduction

In the 20th century, the most common element in the crust of the earth is arsenic. It occupies about 0.00005 % surface of the earth. Arsenic (As) is a carcinogenic and poisonous metalloid that enters the aqueous system via both natural and artificial sources [1]. Many contaminants found in water streams have been identified to be hazardous and damaging to both the environment and human health. Arsenic is a high-priority hazard among them. Inorganic and Organic As species are found mainly in two oxidation states that are as (V) including arsenic acid, arsenic Penta oxide, arsenate, dimethyl arsenic acid (DMAA), and monomethyl arsenic acid (MMAA) in the rocks and soils, water, air, plants, and animals in their natural habitats. As can be released into the environment via volcanic activity, weathering of rocks and minerals, and forest fires, among others. The discharge of arsenic into the environment is also due to anthropogenic activity. Arsenic can be found in wood preservatives, paints, pharmaceuticals, dyes, metals, and semiconductors. Arsenic is also produced as a result of agricultural applications (pesticides, fertilizers), fossil fuel combustion, mining, smelting, landfilling, and other industrial activities [2]–[4]. Humans are affected by arsenic contamination which can cause cerebrovascular and cardiovascular diseases, lung, skin, and bladder disorders as well as gastrointestinal problems. Presence of excess amounts of as (V) in drinking water cause several health issues which engulfed various countries including the United States. In 1993 World Health Organization (WHO), need to protect people against the effects of long-term, chronic exposure to drinking water (WHO, 2001), and modifications in the WHO's arsenic standard for drinking water (WHO, 2001), the United States Environmental Protection Agency (US EPA) has dropped the current maximum contaminants level for arsenic in drinking water from 0.05 mg/L (50 ppb) to 0.01 mg/L (10 ppb), (US EPA, 2003). The standard concentration for As in drinking water is 10 μg/L reported by the latest standards Environmental Protection Agency (EPA) [5]–[7]. To comply with the EPA proposed arsenic standard, numerous smaller drinking water treatment plants are required for additional treatments. Individual ground wells and other small-scale water systems are common in arsenic-endemic areas, and scientists have recently focused on producing techniques that are both cost-effective and practical for their desired purposes. For the removal of As (V) from an aqueous environment, various techniques have been used as Adsorption, Precipitation-coagulation, membrane technology (reverse osmosis and nanofiltration), and so on [7]. But adsorption is becoming an attractive and promising technology among others because of its simplicity, cheaper pollution control method, ease of operation and handling, sludge-free operation, and regeneration capacity.

Iron and aluminum-based adsorbents have been considered one of the best small-scale arsenic removal techniques [6]. For the design of adsorbers, detailed information on equilibrium data is required [8]. The adsorption equilibrium provides basic physicochemical information for evaluating the applicability of sorption operations as a unit operation. The sorption equilibrium is commonly described by an isotherm equation, whose parameters indicate the surface characteristics and affinity of the sorbent at a certain temperature and pH. As a result, for the effective design of adsorption contact processes, an exact mathematical description of the equilibrium isotherm is required [9]. Adsorption is a relatively inexpensive technique for separating a small number of hazardous substances from vast quantities of solution. These advantages have driven numerous researchers to utilize adsorption to remove arsenic from drinking water. The following materials are used as adsorbents for removal from an aqueous environment i.e., Activated alumina, manganese green sand, granular ferric hydroxide, soil, and mud [7], [10]. Table 1. illustrated the different adsorbents along with their maximum adsorption capacities. This article illustrates the adsorption of as (V) by iron (Fe_2O_3) and aluminum (Al_2O_3).

Material And Methods

In the current research work, all the chemicals and reagents were used of analytical grade. $FeCl_3.6H_2O$ (Sigma Aldrich), $Al(NO_3)_3 \cdot 9H_2O$, $Al_2(SO_4)_3 \cdot 18H_2O$, distilled water, urea

($CO(NH_2)_2$),. Iron(III) chloride hexahydrate ($FeCl_3$, $6H_2O$), ammonia hydroxide (NH_4OH), ethanol (C_2H_6O), NaOH, and HCl (37%) were obtained from Merck, KGaA Darmstadt (Germany). Throughout experiments distill water was used [11] [12] [13].

Table 1. Adsorptive removal of as (V) via different adsorbents along with their maximum adsorption capacities (Q_{max}).

S. No.	Adsorbent Type	Q_{max}(mg/g)	References
1.	Zirconium oxide	32.4	[11]
3.	$ZrO(OH)_2$/CNT	124.6	[12]
4.	TiO_2 cluster	124.0	[13]
5.	TiO_2 nanoparticles	150.0	[14]
6.	rGO-TiO_2/Fe_3O_4	150.0	[15]
7.	Alumina/cigarette soot carbon	96.9	[16]
8.	Aluminum-magnesium oxide	912.0	[17]
10.	Ceria-GO	212.0	[18]
11.	Cerium–iron mixed oxide	216.72	[19]
12.	Iron-cerium bimetal oxide	216.72	[20]
13.	Al_2O_3	90	[21]
14.	Iron-manganese oxide	77.0	[22]
15.	GO-$MnFe_2O_4$	207.0	[23]
16.	Fe-Cu binary oxide	82.7	[24]
17.	Al-Mg oxide	133.0	[25]
18.	Akageneite	1.79	[26]
19.	Fe_2O_3	0.616	[27]
20.	Goethite	0.33	[28]
21.	Hydrous ferric oxide	1.34	[29]
22.	Iron oxide-coated sand	0.0055	[30]
23.	Fe(III) loaded resin	0.80	[31]
24.	Ce(IV) doped iron oxide	0.93	[32]
25.	Natural iron ores	0.0053	[33]
26.	Magnet. modified zeolite	0.93	[34]
27.	Fe-hydroxide coated alumina	0.212	[35]
28.	Sand-red mud columns	0.013	[36]
29.	Fly ash	0.0026	[37]

Synthesis of iron oxide nanoparticles (Fe_2O_3-NPs)

The Fe_2O_3-NPs were synthesized via the chemical precipitation method [14][15][16]. Initially, 0.05 M aqueous solution of $FeCl_3.6H_2O$ were prepared in distilled water, stirred magnetically for 40 min at 353 K temperature, and then 1 M NaOH solution was added dropwise until the pH reached the value of 11, and the mixture was heated up to 353 K temperature and finally magnetic stirring for 4 h [18][19][20] The resulting precipitations were collected, centrifuged at 4000 rpm, washed with distilled water and ethanol three times and dried at 353 K, and finally calcined at 973 K temperature for 4 h [21][22][39].

Synthesis of iron oxide nanoparticles (Fe_2O_3-NPs) Process Flow Diagram

Synthesis of aluminum oxide nanoparticles (Al_2O_3-NPs)

The aluminum oxide (Al_2O_3-NPs) was synthesized via a chemical precipitation technique. Initially, $Al_2(SO_4)_3.18H_2O$ and $Al(NO_3)_3.9H_2O$ (10 m.mol/L:0.5 m.mol/L) solutions were prepared in distilled water, respectively.[23][24][25] And then urea $CO(NH_2)_2$ was added to the

solution up to $CO(NH_2)_2$ and Al^{3+} ratio to 100 [26][27]. Then, the mixture was stirred for 30 min. Then heat the mixture to 368 K temperature under vigorous stirring for 4 h.[28][29][30][31] The resulting precipitations were collected, centrifuged at 4000 rpm, washed with distilled water and ethanol three times, and then dried at 333 K and finally, calcined at 973 K temperature for 4 h [32][33][40].

Synthesis of aluminum oxide nanoparticles (Al_2O_3-NPs) Process Flow Diagram

Characterization of synthesized as Fe_2O_3-NPs and Al_2O_3-NPs

The synthesized material (Fe_2O_3-NPs and Al_2O_3-NPs) was characterized by different analytical techniques such as FT-IR and XRD spectroscopic techniques. For FT-IR spectroscopic techniques, the sample (required quantity) was mixed with KBr (IR grade) and then evaluated using an FT-IR spectrometer at room temperature in the 4000–500 cm^{-1} range [34]. The X-ray diffractometer was employed for analysis with the following scanning parameters: CuK radiations, scanning speed of 0.1°/sec, scanning range 2 of 5 to 80°, tube voltage of 40 kV, and current of 20 mA [35].

Adsorption studies of as (v) onto synthesized material as Fe_2O_3-NPs and Al_2O_3-NPs

Batch adsorption experiments were carried out in triplicate to remove as (V) from the aqueous system. For this purpose, a standard solution of as (V) (1000 mg/L) was prepared by dissolving disodium arsenate ($HAsNa_2O_4$) in distilled water [36]. The dilution formulas are described in Equation 1. Were used to prepare the working standards as (V).

$$Cc\,Vc = Cd\,Vd \qquad (1)$$

Where C and V are the concentration and volume, while "c" and "d" are the concentrated and diluted solution, correspondingly.

We Investigated various parameters for the maximum removal of as (V) Using Fe_2O_3-NPs and Al_2O_3-NPs. The parameters include pH, adsorbent dose, temperature, and time. For the effect of pH, 0.5 mg/L As (V) solution was taken in 250 mL of various conical flasks. To adjust pH 0.1 M HCl and NaOH were used in the as (V) solution. 0.2 g adsorbent Fe_2O_3-NPs were added to each conical flask and shaken for 30 minutes at room temperature at speed of 200 rpm. After shaking the supernatant was centrifuged for 15 min and allowed to stable for 10 minutes and then dilute approximately [37][38] The obtained transparent supernatant solution was analyzed using Atomic Adsorption Spectroscopy (AAS). The same procedure was repeated for As (V) removal via Al_2O_3-NPs and determined the amount of as (V) adsorbed onto the synthesized materials by using the following equation (2).

$$q_e\,(mg/g) = \frac{C_o - C_e}{W} \times V \qquad (2)$$

Where, C_o and C_e (mg/g) show the initial and final concentration of as (V), W (g) shows the weight adsorbent as Al_2O_3-NPs and Fe_2O_3-NPs, while V (L) shows the volume of solution. Similarly, using Equation 3. calculated percent adsorption. By plotting, graph pH vs. q_e/% adsorption determined the optimum pH of the solution

$$\%Adsorption = \frac{C_o - C_e}{C_o} \times 100 \qquad (3)$$

For the contact of time, 0.1 L of 0.5 mg/L As(V) solution was taken in 250 mL of various conical flasks with pH 7 and 0.2 g adsorbent Fe_2O_3-NPs was added to each conical flask, and shake the mixture for various intervals of time (2 to 40 min) at room temperature with shaking speed of 200RPM. The remaining steps were the same as those mentioned above, and data was plotted time vs. q_e/percent adsorption. The same procedure was repeated for (V) adsorption onto Al_2O_3-NPs at pH 8. For the effect of temperature, 0.1 L 0.5 mg/L As(V) solution was taken in 250 mL of various conical flasks with pH 7 and 0.2 g adsorbent Fe_2O_3-NPs was added to each conical flask, and shake the mixture for 30 min at various temperatures between 10 and 85 °C with shaking speed of 200 rpm. The remaining steps were the same as mentioned, and data was plotted temperature vs. q_e/percent adsorption. The same procedure was repeated for (V) adsorption onto

Al_2O_3-NPs at pH 8. For the effect of the adsorbent dose, 0.1 L of 0.5 mg/L As (V) solution was taken in 250 mL of various conical flasks with pH 7 and 0.2 g adsorbent Fe_2O_3-NPs was added to each conical flask, and shake the mixture for 30 min at room temperatures with different adsorbate concentration (0.05 g to 1 g) with shaking speed of 200 rpm. The remaining steps were the same as those mentioned above, and data was plotted temperature vs. q_e/percent adsorption. The same procedure was repeated for (V) adsorption onto Al_2O_3-NPs [pH: 8; time: 20 min; room temperature].

Calculation of site energy distribution

The distribution of adsorption site energies, which can be determined from the theoretical isotherm represents the measured equilibrium data, is one of the premises of isotherm models. The following is representation of the general integral equation for the adsorption of arsenic onto Fe_2O_3-NPs and Al_2O_3-NPs:

$$q_e(Cq_e) = \int_{-\infty}^{+\infty} q_h(E, Cq_e)F(E)dE \qquad (4)$$

or

$$F(E) = \frac{-dqe\,(E*)}{dE*} \qquad (5)$$

Where C_e denotes the equilibrium concentration of sorbate in the liquid phase in (mg/L), q_e (C_e) denotes the total solute sorption to the sorbent in (mg/g), q_h (E, C_e) denotes the isotherm over sorption sites with sorption energy E (mg/g), and F(E*) denotes the frequency of sites with homogeneous energies between the solute and solvent for a given sorption site. Since the value of negative infinity (-∞) will not have any physical significance, it is believed that the range of energies is from 0 to infinite (∞) (4).

Because this problem is challenging to solve and because there isn't a single general analytical solution, Condensation approximation, or Cerofolini's asymptotically correct approximation, as indicated in eq. (6) was employed for simplification. Using a variety of isotherm models, including the Freundlich, Langmuir, Langmuir-Freundlich, and Dubinin-Ashtaknov isotherm models, this technique was utilized to determine the estimated site energy distribution.

$$\mathrm{Ce} = \mathrm{Cse}\left(-\frac{E-Es}{RT}\right) = \mathrm{Cse}\left(-\frac{E*}{RT}\right) \quad (6)$$

As is the lowest physically realizable sorption energy (J/mol), R is the universal gas constant (J/mol-K), T is the absolute temperature (K), and E* is the difference between sorption energies at Ce and Cs (J/mol) where Cs is the solute's solubility in the solvent (mg/L).

Results And Discussions

Characterization Of Synthesized Material

The materials such as Fe_2O_3-NPs and Al_2O_3-NPs were synthesized via the chemical precipitation method. By using Fourier Transform Infrared (FT-IR) Spectroscopy, X-Ray Diffraction (XRD) spectroscopy synthesized material was characterized. The FT-IR study of the synthesized Fe_2O_3-NPs yielded results in the 400–4000 cm^{-1} wavenumber region, identifying both the chemical bonds and functional groups (Figure 1.). The synthesized Fe_2O_3-NPs show different peaks in their FTIR spectra at 517, 621, 1020, 1612, and 3435 cm^{-1}. Due to the vibrational intrinsic stretching of the metal-oxygen bond vibrations (in this case, Fe-O), two distinct peaks appeared at 517 cm^{-1} and 621 cm^{-1}, confirming the synthesis of Fe_2O_3-NPs were iron oxide [41], [42]. Due to the asymmetric stretching of Fe-O, a slightly smaller peak at 1020 cm^{-1} was observed. Indicating the bending vibration of absorbed water and surface hydroxyl (-OH) groups, the absorption peaks at 1612 cm^{-1} and 3431 cm^{-1} [43] may have been caused by the usage of NaOH in the synthesis of the Fe_2O_3-NPs [44]–[48]. These results were further confirmed by the previous publication, which indicated that the synthesized of NPs were iron oxide.

Figure 1. illustrates the solid phase FTIR spectra of a- and Al_2O_3-NPs in the 400–4000 cm^{-1} range. As a result, the stretching and bending vibrations of adsorbed water molecules are

responsible for the absorption peaks at 3447 sm^{-1} and 1617 cm^{-1} for amorphous and 3451 cm^{-1}, and 1630 cm^{-1} [49], respectively. In amorphous, the broad extending peak at 811 cm^{-1} is caused by the Al-O vibration of (AlO_4) [50].

The synthesized Fe_2O_3-NPs as shown in Figure 2. were evaluated for structure and crystallinity using X-ray diffraction (XRD) crystallography. The diffraction peak in the XRD pattern of the hydrothermally produced Fe_2O_3-NPs was easily identified as being rhombohedral (hexagonal), which denotes the lattice parameter. Using a graphite crystal, the incident X-ray wavelength was monochromatized at 0.154 nm. The peaks observed at 2θ range of 24.15° (012), 33.10° (104), 35.53° (110), 40.59° (113), 49.49° (024), 54.11° (116), 57.32° (018), 62.4° (214), 63.9° (300), 72.1° (1010) and 75.4° (220), which confirm the crystalline structure corresponding to the Fe_2O_3-NPs [51], [52]. These results were consistent with that of the reported studies. As previously reported, the standard values of the peaks for magnetite and maghemite were found to be 35.43° and 35.62°, respectively. In the current study, the synthesized Fe_2O_3-NPs had a diffraction angle of 35.53° (110), which was closer to the magnetite index than the maghemite index [43], [44]. This result indicated that in the synthesized iron oxide NPs, maghemite lattice predominated over magnetite (Fe_3O_4) lattice. Finally, it is clear from the XRD peaks that the Fe_2O_3-NPs were synthesized.

Figure 2. illustrates the XRD patterns of samples Al_2O_3-NPs. In the case of Al_2O_3-NPs, XRD investigation showed a succession of diffraction peaks at 2 of 32.52, 37.62, 39.63, 45.95, 61.08, and 67.07, which are corresponding to the crystal planes (220), (311), (222), (400), (511), and (440), respectively. Likely related to a pure cubic structure of -Al2O3 were all the diffraction peaks [42], [53].

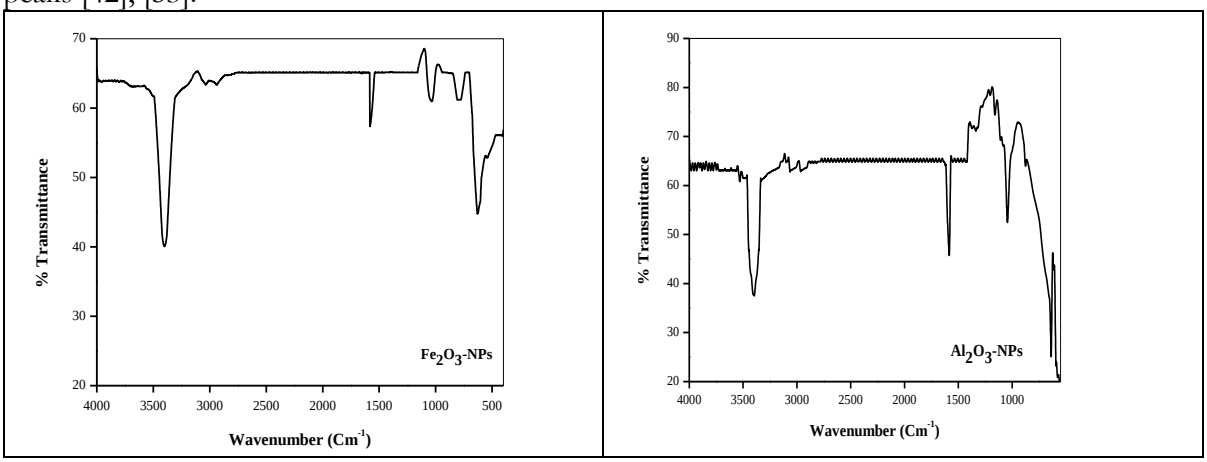

Figure 1. FT-IR spectrum of synthesized materials such as Fe_2O_3-NPs and Al_2O_3-NPs

The synthesized adsorbent as Fe_2O_3-NPs, the adsorption ability was evaluated at various pH values ranging from 1.0 to 11.0 with a (V) concentration of 80 mg/L. The investigations [54], [55] revealed that the adsorption process increased as pH increased. It is obvious that pH significantly affects the amount of as (V) that adhere to the surface of Fe_2O_3-NPs. At pH 7.0, As (V) adsorption was at its highest as shown in Figure 3. Which was considered the optimum adsorption process conditions. At pH 7.0 the as (V) adsorption was observed about 21 mg/g (52.5%), respectively. After the adsorption procedure, the final pH of each solution was measured, and it was found that the final pH of the solution was lower than the initial value. This study shows that as (V) was adsorbed onto Fe_2O_3-NPs using an exchange process. Additional studies, was focused on keeping the pH at 7.0. Furthermore, adsorption of as (V) onto Al_2O_3-NPs was also investigated and the result shows (Figure 3.) that adsorption increased with pH increased up to

pH 8. The maximum adsorption at pH 8 was about 20.5 mg/g and 51.5% and finally, it was considered optimum pH of as (V) onto Al_2O_3-NPs.

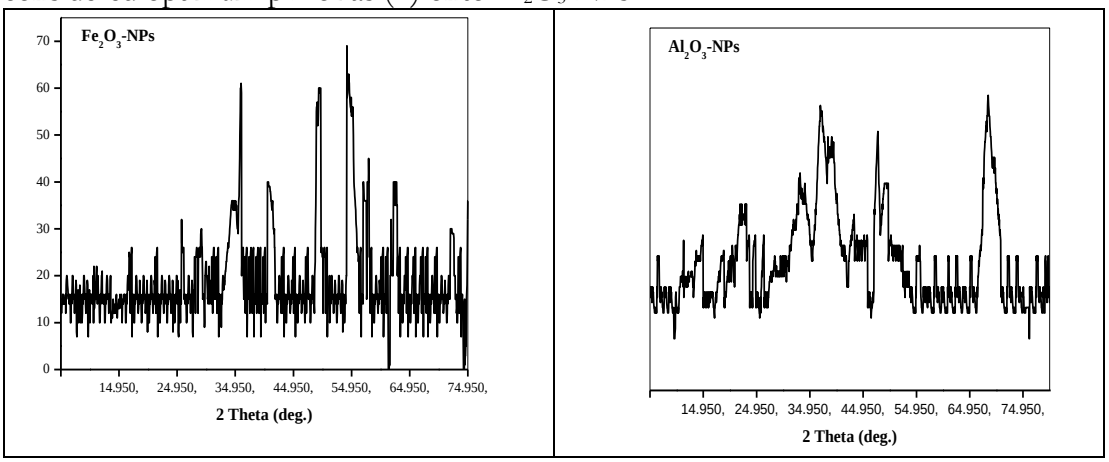

Figure 2. Ft-ir spectrum of synthesized materials as (a) fe_2o_3-nps (b) al_2o_3-n adsorption was studied as (V) onto the synthesized materials as (a) fe_2o_3-nps(b) al_2o_3-nps

The adsorption efficiency of the synthesized material was studied with the influence of various time intervals [56], [57]. It was observed that practically all of the data obtained were comparable indicating that the adsorption process increases with time. Time has a great effect on adsorption. Finally, results show that equilibrium was achieved after 20 min using Fe_2O_3-NPs. At equilibrium, the as (V) adsorption was obtained at about 21.5 mg/g which is 53.75% as shown in Figure 3, respectively. Therefore, the optimum adsorption time for as (V) was considered to be a time of 20 min.

Furthermore, the adsorption efficiency of the Al_2O_3-NPs with various time intervals was investigated. It was observed that practically all of the data (Table 3.5) obtained were comparable, indicating that the adsorption process increases with time. The results show that equilibrium was achieved using Al_2O_3-NPs with about 19.5 mg/g which is 48.75% as shown in Figure 3. Therefore, the optimum adsorption time for as (V) adsorption onto Al_2O_3-NPs was considered to be a time of 20 min.

Adsorption experiments for as (V) adsorption onto Fe_2O_3-NPs was carried out at various temperatures to examine the effect of temperature [58]. It was determined that all of the results (Table 3.5) were varies with s temperature changes. This proves that the Fe_2O_3-NPs adsorption capacity has a significant effect on temperature. The results show that the maximum adsorption using Fe_2O_3-NPs is (V) adsorption with about 20.45 which is 50% at 25°C temperature. Finally, the optimum temperature for an adsorption experiment was considered to 25°C.

Also, Adsorption experiments as (V) adsorption onto Al_2O_3-NPs was carried out at various temperatures to examine the effect of temperature. It was discovered that all of the results were varies with temperature changes. The results show that the maximum adsorption using Al_2O_3-NPs for as (V) adsorption with about 18.75 which is 48.75% at 25°C. Finally, the optimum temperature for an adsorption experiment was considered to 25°C.

The adsorption capability of the Fe_2O_3-NPs was determined using various adsorbate concentrations ranging from 20 mg/L to 100 mg/L. The results indicate that when adsorbate concentration increased the adsorption capacity significantly increased while percent adsorption decreased (Figure 3.). In the adsorption processes, this is the usual behavior. The results show that the maximum adsorption using Fe_2O_3-NPs for as (V) adsorption with about 20 which is 50% at 25°C temperature. The relationship between as(V) concentration and percent adsorption is that a decrease as adsorbent dose increases because the availability of the active sites decreased.

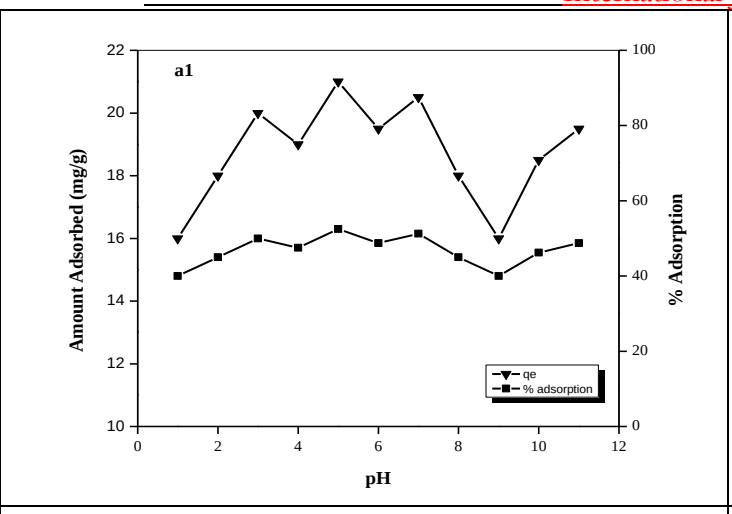
a1
Amount Adsorbed (mg/g)
% Adsorption
pH
qe
% adsorption

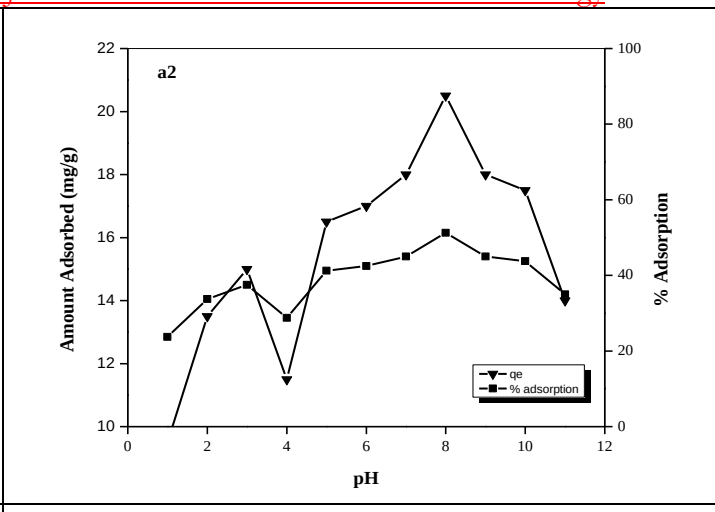
a2
Amount Adsorbed (mg/g)
% Adsorption
pH
qe
% adsorption

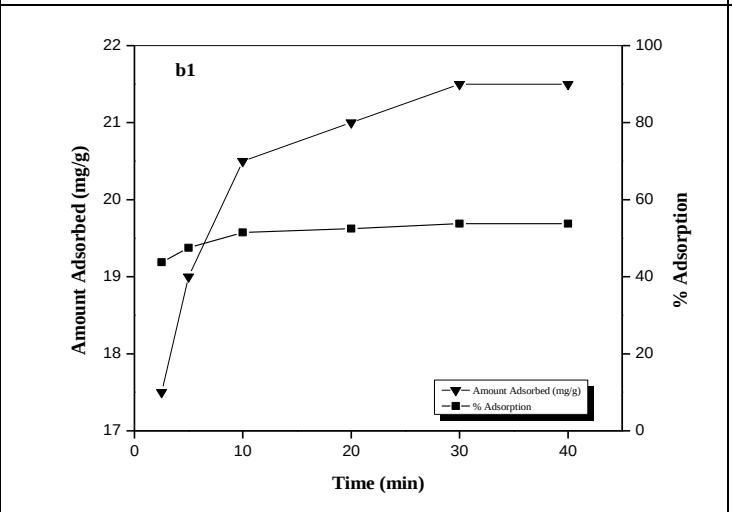
b1
Amount Adsorbed (mg/g)
% Adsorption
Time (min)
Amount Adsorbed (mg/g)
% Adsorption

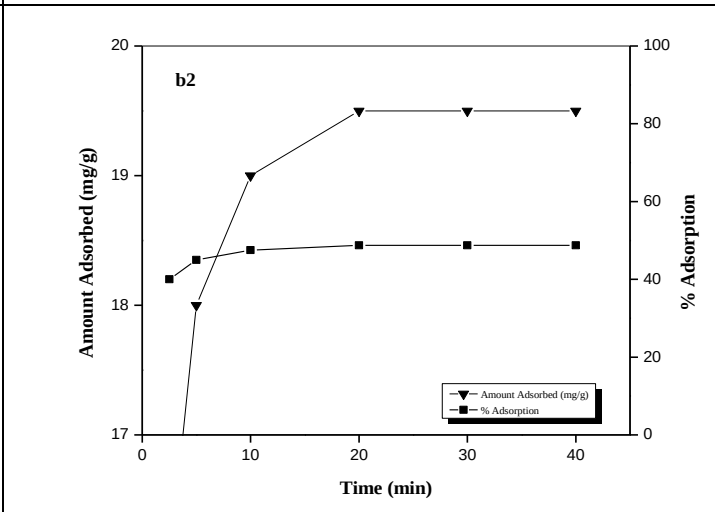
b2
Amount Adsorbed (mg/g)
% Adsorption
Time (min)
Amount Adsorbed (mg/g)
% Adsorption

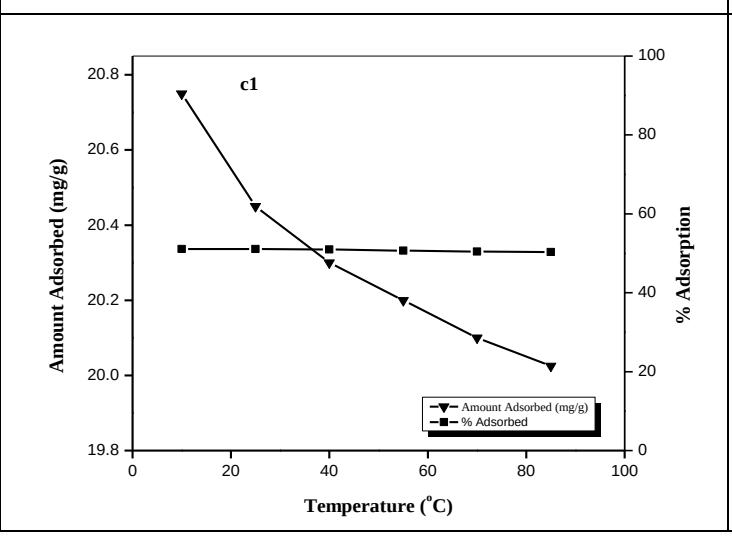
c1
Amount Adsorbed (mg/g)
% Adsorption
Temperature (°C)
Amount Adsorbed (mg/g)
% Adsorbed

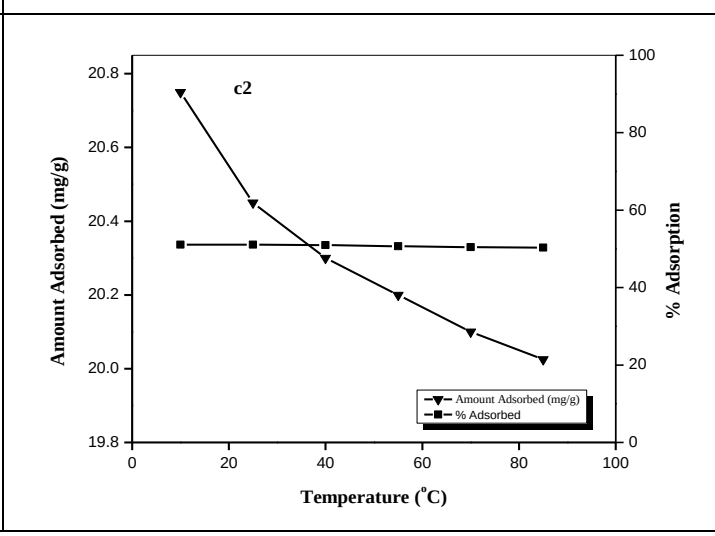
c2
Amount Adsorbed (mg/g)
% Adsorption
Temperature (°C)
Amount Adsorbed (mg/g)
% Adsorbed

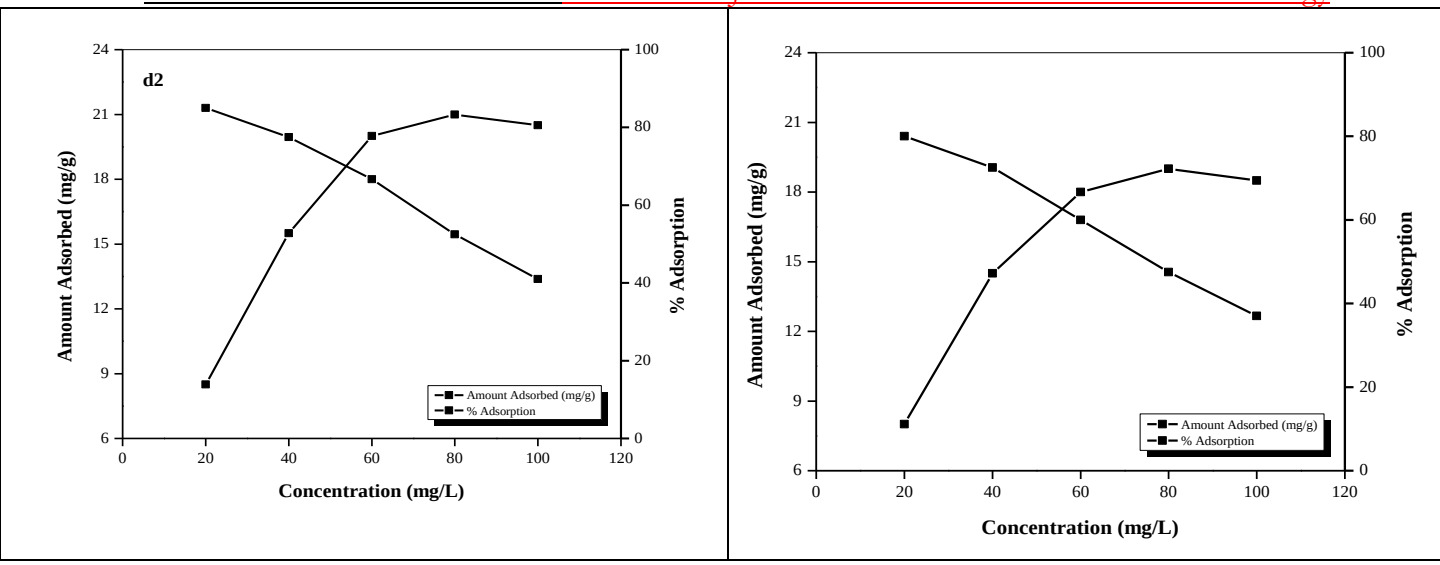

Figure 3. Illustrates the Adsorption of as (V) (onto Fe_2O_3-NPs at (a1) effect of pH (b1) effect of time (c1) effect of temperature (d1) effect of adsorbate concentration) (onto Al_2O_3-NPs at (a2) effect of pH (b2) effect of time (c2) effect of temperature (d2) effect of adsorbate concentration. Also, the Adsorption capability of Al_2O_3-NPs was investigated at various temperatures to examine the effect of temperature. The result shows that the maximum amount of as (V) adsorption at 40 mg/L concentration of as (5) solution. At this concentration, the adsorption was recorded about 15.5 mg/g which is 77.5% at 25°C temperature. Finally, the optimum concentration for as (V) adsorption was considered to be 40 mg/L, respectively (Figure 3).

Application to the real sample

Adsorption of as (V) from actual samples was also examined. Three actual samples, including tap water, well water, and river water were used for this study. According to the findings, all the samples containing 100 mg/L As (V) were used to adsorbed as (V) at the ideal conditions as mentioned above. The result shows in Figure 4. that maximum removal of as (V) was observed in tap water because of minimum interfere species, as interfere species increases the adsorption decreases.

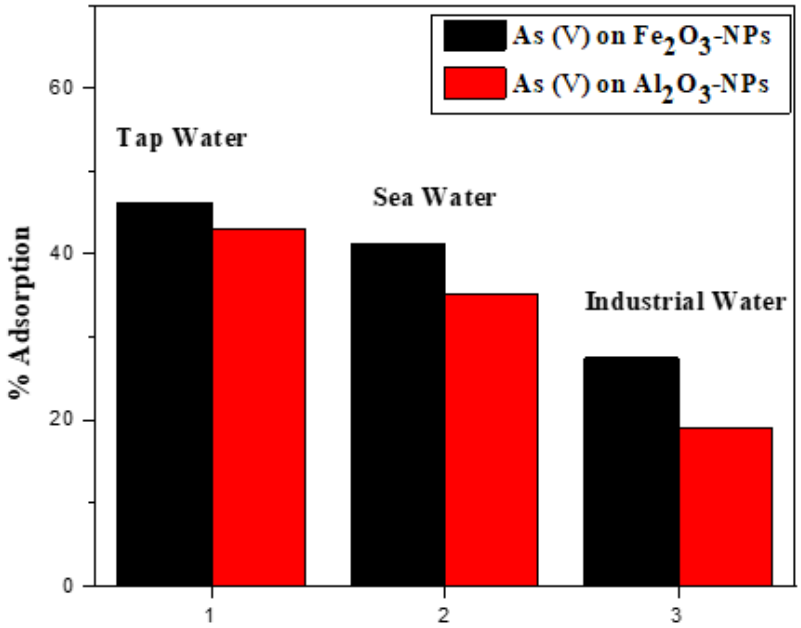

Figure 4. Adsorption of as (v) in real sample

Kinetic Studies

Adsorption models/kinetics, equilibrium, and thermodynamic studies for as (v) adsorption onto Fe_2O_3-NPs and Al_2O_3-NPs

Various theoretical investigations were carried out to illuminate the nature of adsorption and potential adsorption mechanisms [51], [52]. Applied the adsorption data to well-known adsorption equations and models for analysis purposes as:

Pseudo-first-order (PFO) equation; $log(q_e - q_t) = log\ q_e - \frac{K_1 t}{2.303}$ (4)

Pseudo-second order kinetic (PSK) equation; $\frac{t}{q_t} = \frac{t}{q_e} - \frac{1}{K_2 q_e^2}$ (5)

Intraparticle diffusion (IPD) equation; $q_t = K_{int} t^{1/2} + C$ (6)

Dubinin-Radushkevich adsorption (DRA) equation;$q_t = \frac{1}{\beta}\ln(\alpha\beta) + \frac{1}{\beta}\ln t$ (7)

Where qt (mg/g) shows the adsorption capacity at time (t), qt (mg/g) shows the adsorption capacity at equilibrium, K_1(min-1) is the rate constant of pseudo-first-order kinetic adsorption, K_2 (g/mg/min) is the rate constant of the pseudo-second-order kinetic equation, K_{int} (mg/g/$min^{1/2}$) is the rate diffusion equation constant, C is the intercept related to the thickness of the boundary layer and α and β is the Elovich coefficients shows the initial rate (mg/g.min), the extent of the surface coverage and activation energy for adsorption. Based on high values of the linear regression coefficient (R2), as seen in Table 2. the results indicate that the data was successfully fitted in the pseudo-second-order kinetic model. As a result, it can be seen that the rate of adsorption was directly related to the square of the number of empty spots and that the ionic interaction or ion-exchange mechanism appears to be in charge of the adsorption process. The mechanism of pseudo-second-order kinetic adsorption primarily consists of two steps: the external diffusion step, in which as (V) molecules move from the bulk of the solution to the external surface of Fe_2O_3-NPs and Al_2O_3-NPs, and the adsorption step in which adsorbate molecules adhere to the adsorbent surface, likely as a result of ionic interaction.

The following model/equation [52] was used for the equilibrium analysis:

Freundlich model/equation; $logq_e = logK_F + \frac{1}{n} logC_e$ (8)

Langmuir model equation; $\frac{C_e}{q_e} = \frac{1}{K_L} + \frac{a_L C_e}{K_L}$ (9)

Temkin model equation; $q_e = B_T lnA_T + B_T lnC_e$ (10)

Dubinin-Radushkevich models equation; $lnq_e = lnQ_m - K\varepsilon^2$ (11)

Where, C_0 (mg/L) and C_e (mg/L) stand for the initial and equilibrium concentrations, respectively. Q_e (mg/g) and q_m (mg/g) stand for maximum adsorption capacity and equilibrium capacity, respectively. The R_L separation factor, which has no dimensions, is used to assess the viability of adsorption within a certain concentration range. The binding energy constants for the Langmuir and Freundlich models are denoted by the letters k_L and k_F, respectively. The constant A_T (L/g) is the equilibrium binding constant corresponding to the maximum binding energy, Q_m (mg/g) is the theoretical saturation capacity, K (mol^2/kJ^2) is a constant for the adsorption energy, and B_T (mg/g) is related to the adsorption capacity of an adsorbent. The Polanyi potential represents by ε, which is calculated by the following equation/model.

$$\varepsilon = RTln\left(1 + \frac{1}{C_e}\right) \quad (12)$$

Based on high values of the linear regression coefficient (R^2), as shown in Table 3. the data are better suited in the Freundlich adsorption model for Fe_2O_3-NPs, while for Al_2O_3-NPs the data are more fitted to Temkin model/equation. Because this model works well for a very heterogeneous surface, it is reasonable to assume a heterogeneous surface with a non-uniform distribution of heat of adsorption throughout the surface. When the adsorption center of an adsorbent is fully used, the Freundlich equation application predicts that the adsorption energy

will drop exponentially. The maximal adsorption capacity (L/g) and bonding strength (L/g), respectively, are correlated with KL and aL. K_L/a_L is the numerical equivalent of the theoretical monolayer adsorption capacity (Q_o, mg/g).

$$Q_o = \frac{K_L}{a_L} \qquad (13)$$

The separation factor (RL)(g/L), may be used to describe the fundamental properties of the Langmuir adsorption model; where Ci (mg/L) is the initial concentration of as (5) in the solution. The value of R_L shows whether the isotherm is irreversible (RL = 0), linear (RL = 1), unfavorable (RL > 1), or favorable (0< RL< 1). Advantageous adsorption is indicated by R_L values between 0 and 1. The current study values of RL are greater than 0 and less than 1, which supported the finding that (5) adsorption onto Fe_2O_3-NPs and Al_2O_3-NPs is favorably shown in Figure 5.

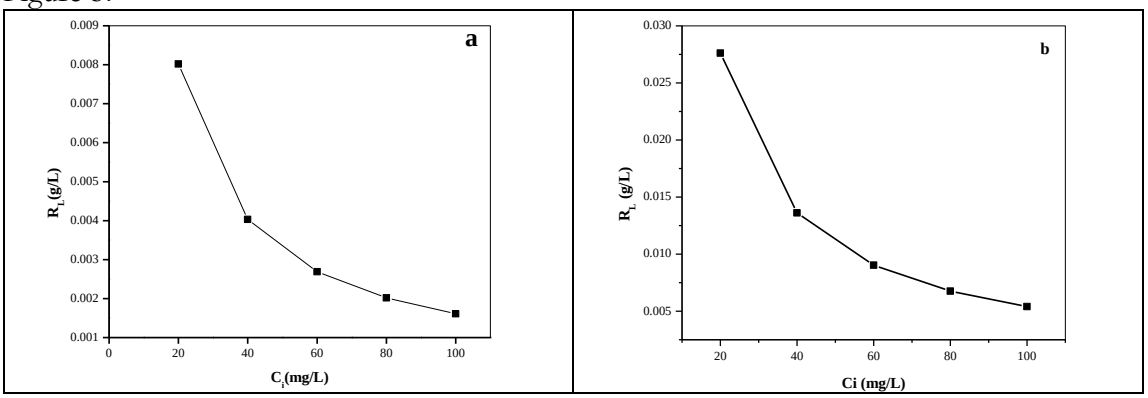

Figure. 5. R_L values affect the (5) concentration of (a) Fe_2O_3-NPs (b) FAl_2O_3-NPs

The following equation has been used to calculate the thermodynamic data such as change in Gibbs free energy (Go), change enthalpy (Ho), and change entropy (So) for the adsorption of arsenic.

$$K_D = \frac{q_e}{C_e} \quad (14)$$

K_D (L/g), which stands for adsorption distribution constant The Van't Hoff equation's linear version provides the K_D and temperature (T) relation.

$$lnK_D = -\frac{\Delta H^o}{RT} + \frac{\Delta S^o}{R} \quad (15)$$

The ΔG° value can be found by using the correlation as;

$$\Delta G^o = \Delta Ho - T\Delta So \qquad (16)$$

G°, H°, and S° were calculated based on the data gathered and are given in Table 4. The adsorption process is non-spontaneous, endothermic, and involves the ion-exchange mechanism; as shown by the positive G° value. Additionally, the strong adsorption capability at low temperatures is demonstrated by the reduction in G° values as temperature rises. Raising the temperature causes the as (V) molecules to travel more quickly, causing them to flee from the solid medium and enter the liquid one. As a result, there will be less (V) adsorption. K_D values also suggested a similar trend. The endothermic character of the adsorption process is demonstrated by the positive values of H° shown by Fe_2O_3-NPsand negative values shown by Al_2O_3-NPs which confirm that the reaction is exothermic, confirming that the adsorption might be more advantageous at lower temperatures and establishing the physisorption phenomena. The positive value of S° determined during the sorption of as (V) onto synthesized material demonstrates the enhanced randomness at the solid-liquid interface (a: 0.0073211; b: 8.44 × 10^{-3}kJ/K.mol).

Analysis of adsorption site energy distribution

The energy of the adsorption site was determined by calculating the adsorption isotherms of arsenic adsorption onto Al_2O_3-NPs and Fe_2O_3-NPs at temperatures of 283, 298, 313, 328, 343, 358 K, as shown in Figure 2, With the increase of temperature, the adsorption capacity of

synthesized materials was decreased accordingly. The results reveal that arsenic adsorption on synthesized Fe_2O_3-NPs was exothermic, and it was the same as the adsorption process of arsenic on Al_2O_3-NPs. The results were shown in Table 33 as being well matched by the Langmuir-Freundlich model (Eq. (14)) for the arsenic adsorption process on Fe_2O_3-NPs with a high R^2 of 0.99537, while arsenic adsorption onto Al_2O_3-NP R^2 value is more fitted for Temkin-Langmuir model. The same n values obtained at different temperatures demonstrate that the surface heterogeneity was constant over the whole temperature range under investigation. The site energy E can be calculated using isotherm modeling and Equation 6. Figure 30 and Figure 31 show the equilibrium Arsenic adsorption capacity at various temperatures. The E* value decreases as arsenic adsorption on synthesized materials increases. This suggests that arsenic was first adsorbed to high-energy adsorbed sites and then to low-energy adsorbed sites.

In Figure. 32 the energy distribution of the arsenic adsorption sites for QM, and at various temperatures on synthesized materials calculated using the Langmuir-Freundlich model (Eq. (9)) is depicted. The site energy was used to describe the forces that interact between arsenic and synthesized materials to comprehend the surface energy heterogeneity and adsorption affinity of Al_2O_3-NPs and Fe_2O_3-NPs at various temperatures. The surface energy inhomogeneity of synthesized materials might be understood by the width of the site energy distribution. Following the weighted mean formula (), the average site energies (E) of arsenic adsorption on Al_2O_3-NPs and Fe_2O_3-NPs were determined.

$$\cup (E*) = \frac{\int_{-\infty}^{+\infty} E*.F(E*)dE*}{\int_{-\infty}^{+\infty} F(E*)dE*} \quad (7)$$

Combining the equations (5, 6, 7) would get the weighted mean.

$$U(E*) = \frac{RTnx}{\alpha} \ln(\beta C + 1) \quad (8)$$

The average site energy and adsorption affinity generally exhibited a positive association. By computing Equation 8., the energy of the adsorption sites for as adsorption onto Fe_2O_3-NPs at 298, 313, 343 K calculating to 35.1, 32.2, and 26 kJ/mol, while as adsorption onto Fe_2O_3-NPs at 298, 313, 343 K calculating to 32.3, 26.3 and 21.1 kJ/mol respectively. The average site energy of synthesized material was affected by solution temperature in the following ways. The primary mechanism of arsenic adsorption of its interactions with adsorbent. This was the polar interaction between electron-rich (donors) and electron-deficient (acceptors). When arsenic was adsorbing on Al_2O_3-NPs and Fe_2O_3-NPs, the -acceptors were regarded as electron-deficient -systems (arsenic), and the -donor was acting as an electron-rich aromatic -system (Al_2O_3-NPs and Fe_2O_3-NPs). The intensity of -electron donors and -receptors would typically rise with a compound's increased polarizability and associated structure. Temperature improves the polarizability of static dipoles as well as making the adsorbent (Al_2O_3-NPs and Fe_2O_3-NPs) and the adsorbate (arsenic) more active donors and acceptors of electrons and increasing the affinity of adsorption. It showed that the average site energy increases little as the temperature rises.

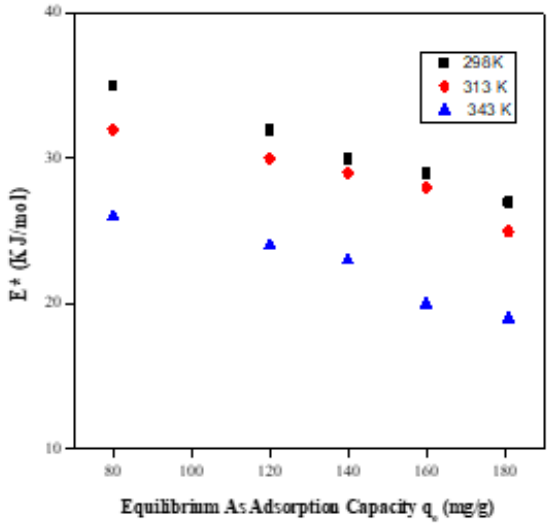

Figure.30. Site energy with corresponding distribution of As on Fe_2O_3-NPs at various temperature, E*; Site energy, as; Arsenic, experiment was trice and calculated mean value of a representative experiment¤

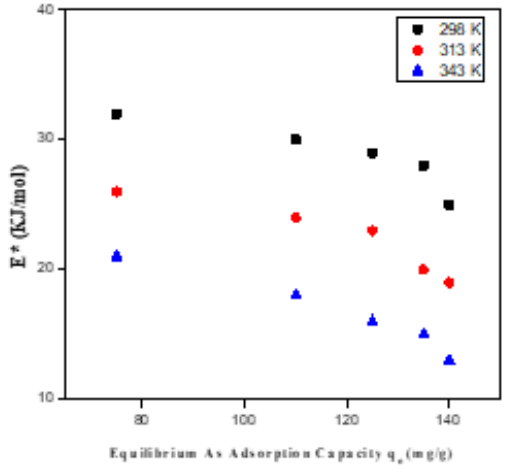

Figure.31. Site energy with corresponding distribution of As on Al_2O_3-NPs at various temperature, E*; Site energy, as; Arsenic, experiment was trice and calculated mean value of a representative experiment¤

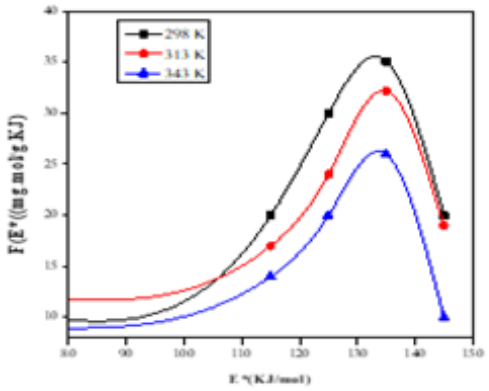

Figure 32. Site energy with corresponding distribution of As on Fe_2O_3-NPs at various temperature, E*; Site energy, as; Arsenic, experiment was trice and calculated mean value of a representative experiment¤

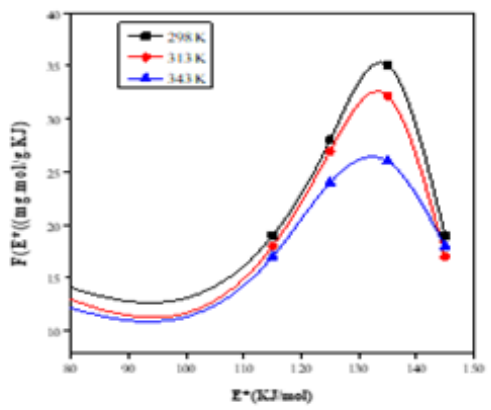

Figure 33. Site energy with corresponding distribution of As on Al_2O_3-NPs at various temperature, E*; Site energy, as; Arsenic, experiment was trice and calculated mean value of a representative experiment¤

Table.2. Kinetics equation/model parameters for adsorption isotherm of as (5) onto Fe2O3-NPs and Fe2O3-NPs.

Kinetics equation	Parameters	Unit	Values (Fe_2O_3)	Values (Al_2O_3)
PF order equation	q_e (Experimental)	mg/g	21.51	19.50
	q_e (Theoretical)	mg/g	21.5	19.51
	K_1	1/min	-0.03137	-0.01725
	R^2	-	0.23326	-0.05038
PS order equation	q_e (Experimental)	mg/g	21.5	19.5
	q_e (Theoretical)	mg/g	21.901	19.79
	K_2	g/mg.min	0.067	0.11
	H	mg/g.min	30.97	41.83
	R^2	-	0.99994	0.99993
IPD equation	K_{int}	mg/g.$min^{1/2}$	0.78778	0.62408
	C	-	17.11359	16.16468
	R^2	-	0.80057	0.62154
Elovich equation	A	mg/g.min	4.091	4.03
	β	mg/g	0.6920	0.8422
	R^2	-	0.9318	0.80466

Table 3. Kinetics equation/model parameters for adsorption isotherm of as (5) onto Fe_2O_3-NPs and Fe_2O_3-NPs.

Kinetics equation	Parameters	Unit	Values (Fe_2O_3)	Values (Al_2O_3)
Freundlich equation	K_f (Experimental)	mg/g	21.5	19.5
	K_f (Theoretical)	mg/g	7.034	6.014
	1/n	1/min	0.29898	0.30558
	N	L/g	3.345	3.272
	R^2	-	0.81366	0.80645
Langmuir equation	q_e (Experimental)	mg/g	22.5	18.5
	q_e (Theoretical)	mg/g	22.19	27.538
	K_L	L/g	6.182	1.861
	R_L	…	0.00161-0.00802	0.0054-0.02761
	aL	L/mg	0.2786	0.06758
	R^2	-	0.99537	0.91973
Temkin equation	B_T (experimental)	mg/g	21.5	19.5
	B_T (calculated)	mg/g	13.7268	11.98498
	A_T	L/g	-4.195	-0.39676
	B_T	J/mol	180.49	206.72
	R^2	-	0.98636	19.5
Dubinin-Radushkevich (D-R) equation	Q_m(experimental)	mg/g.min	21.5	19.5

	Q_m(calculated)	mg/g	19.85	23.05
	K	mol^2/kJ^2	1.516×10^{-5}	-28.95715
	R^2	-	0.9362	0.88761

Table 4. Some thermodynamic parameters of as (V) adsorption onto (a) Fe_2O_3-NPs and (b) Al_2O_3-NPs

Temperature (Kelvin)	ΔG° (a) (kJ/mol)	ΔG° (b) (kJ/mol)	ΔH° (kJ/mol)		ΔS° (kJ/K.mol)	
283	1.573	1990.13	(a) 5.7×10^{-4}	(b) -0.49271	(a) 0.0073211	(b) 8.44×10^{-3}
298	1.609	2027.42				
313	1.634	2052.3				
328	1.659	2064.31				
343	1.684	2084.28				
358	1.699	2104.73				

Conclusion

The synthesized iron oxide nanoparticle (Fe_2O_3-NPs) and aluminum oxide nanoparticle (Al_2O_3-NPs) was synthesized through the precipitation method and found to be efficient removal of as (V) from an aqueous medium. The results show that as (V) was the adsorption process was affected by pH, contact of time, temperature, and initial concentration of adsorbate dose. The maximum removal of as (V) was obtained for Fe_2O_3-NPs at pH: 7, temperature: 25oC, initial concentration of as (V): 40 mg/L, and contact of time: 30 min, which confirms the existence of interaction between Fe_2O_3-NPs and as (V). Besides, the maximum removal of as (V) was obtained for Al_2O_3-NPs at pH: 8, temperature: 25°C, initial concentration of as (V): 40 mg/L, and contact of time: 20 min, which confirms the existence of interaction between Fe_2O_3-NPs and as (V). The synthesis of Fe_2O_3-NPs and Al_2O_3-NPs was confirmed via different analytical techniques such as FT-IR and XRD spectroscopy. Various kinetic and isotherms were investigated in the current study. The result indicated that the obtained data for Fe_2O_3-NPs was more liked to Pseudo second order kinetic and Langmuir model/equation, while Al_2O_3-NPs shows Pseudo second order kinetic and Temkin model/equation, which confirms the interaction among as (V) and adsorbents. Thermodynamic parameters were also investigated which shows the non-spontaneous and endothermic. Thus, both nanoparticles govern as (V) adsorption. However, Fe_2O_3-NPs perform better adsorption as compared to Al_2O_3-NPs of as (V). Furthermore, both materials can be used to reduce the amount of as (V) in wastewater to levels lower than those recommended by WHO and USEPA. The adsorption process was found very quick which boosts industrial application.

References

[1] H. F. Bakhat et al., "Genotypic Differences Among the Rice Genotypes to Arsenic Stress Cultivated Under Two Water Regimes: With an Inference to Human Health," J. Plant Growth Regul. 2021 412, vol. 41, no. 2, pp. 558–568, Mar. 2021, doi: 10.1007/S00344-021-10321-6.

[2] I. Carabante, Arsenic (V) Adsorption on Iron Oxide: Implications for Soil Remediantion and Water Purification, no. V. 2012.

[3] A. Figoli et al., "Arsenic-contaminated groundwaters remediation by nanofiltration," Sep. Purif. Technol., vol. 238, May 2020, doi: 10.1016/J.SEPPUR.2019.116461.

[4] M. Vaclavikova, G. P. Gallios, S. Hredzak, and S. Jakabsky, "Removal of arsenic from water streams: An overview of available techniques," Clean Technol. Environ. Policy,

vol. 10, no. 1, pp. 89–95, 2008, doi: 10.1007/s10098-007-0098-3.

[5] S. I. Siddiqui and S. A. Chaudhry, "Iron oxide and its modified forms as an adsorbent for arsenic removal: A comprehensive recent advancement," Process Saf. Environ. Prot., vol. 111, pp. 592–626, 2017, doi: 10.1016/J.PSEP.2017.08.009.

[6] F. Akhlaghian, B. Souri, and Z. Mohamadi, "Nanostructured Fe2 O3/Al2 O3 adsorbent for removal of As (V) from water," Adv. Environ. Technol., vol. 3, no. 2, pp. 67–75, 2017, doi: 10.22104/AET.2017.2003.1099.

[7] Y. Jeong, M. Fan, S. Singh, C. L. Chuang, B. Saha, and J. Hans van Leeuwen, "Evaluation of iron oxide and aluminum oxide as potential arsenic(V) adsorbents," Chem. Eng. Process. - Process Intensif., vol. 46, no. 10, pp. 1030–1039, Oct. 2007, doi: 10.1016/J.CEP.2007.05.004.

[8] S. Kundu and A. K. Gupta, "Analysis and modeling of fixed bed column operations on As(V) removal by adsorption onto iron oxide-coated cement (IOCC)," J. Colloid Interface Sci., vol. 290, no. 1, pp. 52–60, Oct. 2005, doi: 10.1016/J.JCIS.2005.04.006.

[9] S. Kundu and A. K. Gupta, "Arsenic adsorption onto iron oxide-coated cement (IOCC): Regression analysis of equilibrium data with several isotherm models and their optimization," Chem. Eng. J., vol. 122, no. 1–2, pp. 93–106, Sep. 2006, doi: 10.1016/J.CEJ.2006.06.002.

[10] L. Hao, M. Liu, N. Wang, and G. Li, "A critical review on arsenic removal from water using iron-based adsorbents," RSC Adv., vol. 8, no. 69, pp. 39545–39560, Nov. 2018, doi: 10.1039/C8RA08512A.

[11] H. Cui, Q. Li, S. Gao, and J. K. Shang, "Strong adsorption of arsenic species by amorphous zirconium oxide nanoparticles," J. Ind. Eng. Chem., vol. 18, no. 4, pp. 1418–1427, 2012, doi: 10.1016/j.jiec.2012.01.045.

[12] D. Liu et al., "As(III) and As(V) adsorption on nanocomposite of hydrated zirconium oxide coated carbon nanotubes," J. Colloid Interface Sci., vol. 511, pp. 277–284, 2018, doi: 10.1016/j.jcis.2017.10.004.

[13] H. Gomaa et al., "Highly-efficient removal of AsV, Pb2+, Fe3+, and Al3+ pollutants from water using hierarchical, microscopic TiO2 and TiOF2 adsorbents through batch and fixed-bed columnar techniques," J. Clean. Prod., vol. 182, pp. 910–925, 2018, doi: 10.1016/j.jclepro.2018.02.063.

[14] B. F. Urbano, I. Villenas, B. L. Rivas, and C. H. Campos, "Cationic polymer-TiO2 nanocomposite sorbent for arsenate removal," Chem. Eng. J., vol. 268, pp. 362–370, 2015, doi: 10.1016/j.cej.2015.01.068.

[15] P. Benjwal, M. Kumar, P. Chamoli, and K. K. Kar, "Enhanced photocatalytic degradation of methylene blue and adsorption of arsenic(III) by reduced graphene oxide (rGO)–metal oxide (TiO2/Fe3O4) based nanocomposites," RSC Adv., vol. 5, no. 89, pp. 73249–73260, Aug. 2015, doi: 10.1039/C5RA13689J.

[16] H. Chen, J. Li, X. Wu, and X. Wang, "Synthesis of alumina-modified cigarette soot carbon as an adsorbent for efficient arsenate removal," Ind. Eng. Chem. Res., vol. 53, no. 41, pp. 16051–16060, 2014, doi: 10.1021/ie503057g.

[17] W. Li et al., "Extremely high arsenic removal capacity for mesoporous aluminium magnesium oxide composites," Environ. Sci. Nano, vol. 3, no. 1, pp. 94–106, Feb. 2016, doi: 10.1039/C5EN00171D.

[18] T. S. Sakthivel, S. Das, C. J. Pratt, and S. Seal, "One-pot synthesis of a ceria-graphene oxide composite for the efficient removal of arsenic species," Nanoscale, vol. 9, no. 10, pp. 3367–3374, 2017, doi: 10.1039/c6nr07608d.

[19] B. Chen et al., "Nanocasted synthesis of ordered mesoporous cerium iron mixed oxide and its excellent performances for As(v) and Cr(vi) removal from aqueous solutions,"

Dalt. Trans., vol. 43, no. 28, pp. 10767–10777, 2014, doi: 10.1039/c4dt01101e.

[20] Z. Wen et al., "Facile inverse micelle fabrication of magnetic ordered mesoporous iron cerium bimetal oxides with excellent performance for arsenic removal from water," J. Hazard. Mater., vol. 383, no. July 2019, p. 121172, 2020, doi: 10.1016/j.jhazmat.2019.121172.

[21] N. Inchaurrondo et al., "Synthesis and adsorption behavior of mesoporous alumina and Fe-doped alumina for the removal of dominant arsenic species in contaminated waters," J. Environ. Chem. Eng., vol. 7, no. 1, 2019, doi: 10.1016/j.jece.2019.102901.

[22] D. Ociński, I. Jacukowicz-Sobala, P. Mazur, J. Raczyk, and E. Kociołek-Balawejder, "Water treatment residuals containing iron and manganese oxides for arsenic removal from water - Characterization of physicochemical properties and adsorption studies," Chem. Eng. J., vol. 294, pp. 210–221, 2016, doi: 10.1016/j.cej.2016.02.111.

[23] S. Kumar, R. R. Nair, P. B. Pillai, S. N. Gupta, M. A. R. Iyengar, and A. K. Sood, "Graphene oxide-MnFe2O4 magnetic nanohybrids for efficient removal of lead and arsenic from water," ACS Appl. Mater. Interfaces, vol. 6, no. 20, pp. 17426–17436, 2014, doi: 10.1021/am504826q.

[24] Q. Zhang et al., "Efficient phosphate sequestration for water purification by unique sandwich-like MXene/magnetic iron oxide nanocomposites," Nanoscale, vol. 8, no. 13, pp. 7085–7093, 2016, doi: 10.1039/c5nr09303a.

[25] F. Xiao, L. Fang, W. Li, and D. Wang, "One-step synthesis of aluminum magnesium oxide nanocomposites for simultaneous removal of arsenic and lead ions in water," RSC Adv., vol. 5, no. 11, pp. 8190–8193, 2015, doi: 10.1039/c4ra13146k.

[26] E. A. Deliyanni, D. N. Bakoyannakis, A. I. Zouboulis, and K. A. Matis, "Sorption of As(V) ions by akaganéite-type nanocrystals," Chemosphere, vol. 50, no. 1, pp. 155–163, 2003, doi: 10.1016/S0045-6535(02)00351-X.

[27] J. Youngran, M. FAN, J. Van Leeuwen, and J. F. Belczyk, "Effect of competing solutes on arsenic(V) adsorption using iron and aluminum oxides," J. Environ. Sci., vol. 19, no. 8, pp. 910–919, 2007, doi: 10.1016/S1001-0742(07)60151-X.

[28] K. A. Matis, M. Lehmann, and A. I. Zouboulis, "Modelling Sorption of Metals from Aqueous Solution onto Mineral Particles: The Case of Arsenic Ions and Goethite Ore," Nat. Microporous Mater. Environ. Technol., pp. 463–472, 1999, doi: 10.1007/978-94-011-4499-5_35.

[29] J. A. Wilkie and J. G. Hering, "Adsorption of arsenic onto hydrous ferric oxide: Effects of adsorbate/adsorbent ratios and co-occurring solutes," Colloids Surfaces A Physicochem. Eng. Asp., vol. 107, pp. 97–110, 1996, doi: 10.1016/0927-7757(95)03368-8.

[30] O. S. Thirunavukkarasu, T. Viraraghavan, and K. S. Subramanian, "Arsenic removal from drinking water using iron oxide-coated sand," Water. Air. Soil Pollut., vol. 142, no. 1–4, pp. 95–111, Jan. 2003, doi: 10.1023/A:1022073721853.

[31] I. Rau, A. Gonzalo, and M. Valiente, "Arsenic(V) adsorption by immobilized iron mediation. Modeling of the adsorption process and influence of interfering anions," React. Funct. Polym., vol. 54, no. 1–3, pp. 85–94, 2003, doi: 10.1016/S1381-5148(02)00184-0.

[32] E. Vences-Alvarez, L. F. Chazaro-Ruiz, and J. R. Rangel-Mendez, "New bimetallic adsorbent material based on cerium-iron nanoparticles highly selective and affine for arsenic(V)," Chemosphere, vol. 297, Jun. 2022, doi: 10.1016/J.CHEMOSPHERE.2022.134177.

[33] A. Q. Memon et al., "Experimental investigations of arsenic adsorption from contaminated water using chemically activated hematite (Fe2O3) iron ore," Environ.

Sci. Pollut. Res., vol. 28, no. 10, pp. 12898–12908, 2021, doi: 10.1007/s11356-020-11208-x.

[34] J. bo Huo, G. Yu, and J. Wang, "Magnetic zeolitic imidazolate frameworks composite as an efficient adsorbent for arsenic removal from aqueous solution," J. Hazard. Mater., vol. 412, no. February, p. 125298, 2021, doi: 10.1016/j.jhazmat.2021.125298.

[35] Y. Xu, Y. Yin, M. Guo, G. Xu, L. Li, and C. Liu, "Enhanced removal of arsenic from aqueous solution by novel red mud porous beads: batch and column experiments," Water Supply, vol. 22, no. 4, pp. 3982–3992, 2022, doi: 10.2166/ws.2022.028.

[36] S. A. Khan and M. A. Imteaz, "Batch experiments on arsenic removal efficiencies through adsorption using synthetic and natural sand samples," Int. J. Environ. Sci. Technol., vol. 18, no. 8, pp. 2357–2364, 2021, doi: 10.1007/s13762-020-02999-0.

[37] A. F. Bertocchi, M. Ghiani, R. Peretti, and A. Zucca, "Red mud and fly ash for remediation of mine sites contaminated with As, Cd, Cu, Pb and Zn," J. Hazard. Mater., vol. 134, no. 1–3, pp. 112–119, 2006, doi: 10.1016/j.jhazmat.2005.10.043.

[38] W. Li, "Extremely high arsenic removal capacity for mesoporous aluminium magnesium oxide composites," Environ. Sci. Nano, vol. 3, no. 1, pp. 94–106, 2016.

[39] A. Lassoued, B. Dkhil, A. Gadri, and S. Ammar, "Control of the shape and size of iron oxide (α-Fe2O3) nanoparticles synthesized through the chemical precipitation method," Results Phys., vol. 7, pp. 3007–3015, 2017, doi: 10.1016/j.rinp.2017.07.066.

[40] X. Su, S. Chen, and Z. Zhou, "Synthesis and characterization of monodisperse porous α-Al 2 O 3 nanoparticles," Appl. Surf. Sci., vol. 258, no. 15, pp. 5712–5715, May 2012, doi: 10.1016/J.APSUSC.2012.02.067.

[41] M. Nowsath Rifaya, T. Theivasanthi, and M. Alagar, "Chemical Capping Synthesis of Nickel Oxide Nanoparticles and their Characterizations Studies," Nanosci. Nanotechnol., vol. 2, no. 5, pp. 134–138, 2012, doi: 10.5923/j.nn.20120205.01.

[42] M. Arakha et al., "Antimicrobial activity of iron oxide nanoparticle upon modulation of nanoparticle-bacteria interface," Sci. Rep., vol. 5, no. October, 2015, doi: 10.1038/srep14813.

[43] B. Stephen Inbaraj, T. Y. Tsai, and B. H. Chen, "Synthesis, characterization and antibacterial activity of superparamagnetic nanoparticles modified with glycol chitosan," Sci. Technol. Adv. Mater., vol. 13, no. 1, 2012, doi: 10.1088/1468-6996/13/1/015002.

[44] S. W. Hwang, A. Umar, G. N. Dar, S. H. Kim, and R. I. Badran, "Synthesis and characterization of iron oxide nanoparticles for phenyl hydrazine sensor applications," Sens. Lett., vol. 12, no. 1, pp. 97–101, 2014, doi: 10.1166/sl.2014.3224.

[45] P. Sharma, R. Kumar, S. Chauhan, D. Singh, and M. S. Chauhan, "Facile growth and characterization of α-Fe2O3 nanoparticles for photocatalytic degradation of methyl orange," J. Nanosci. Nanotechnol., vol. 14, no. 8, pp. 6153–6157, 2014, doi: 10.1166/JNN.2014.8734.

[46] P. Saharan, G. R. Chaudhary, S. K. Mehta, and A. Umar, "Removal of water contaminants by iron oxide nanomaterials," J. Nanosci. Nanotechnol., vol. 14, no. 1, pp. 627–643, 2014, doi: 10.1166/jnn.2014.9053.

[47] P. R. Patil and S. S. Joshi, "Synthesis of α-Fe2O3 nanocubes," Synth. React. Inorganic, Met. Nano-Metal Chem., vol. 37, no. 6, pp. 425–429, Jul. 2007, doi: 10.1080/15533170701465960.

[48] S. Wang, X. Li, S. Wang, Y. Li, and Y. Zhai, "Synthesis of γ-alumina via precipitation in ethanol," Mater. Lett., vol. 62, no. 20, pp. 3552–3554, Jul. 2008, doi: 10.1016/J.MATLET.2008.03.048.

[49] A. Afkhami, M. Saber-Tehrani, and H. Bagheri, "Simultaneous removal of heavy-metal

ions in wastewater samples using nano-alumina modified with 2,4-dinitrophenylhydrazine," J. Hazard. Mater., vol. 181, no. 1–3, pp. 836–844, Sep. 2010, doi: 10.1016/J.JHAZMAT.2010.05.089.

[50] B. P. Jacob and P. Laneesh, "Structural changes, magnetic properties and dielectric behaviour of Tb3+ doped Ni-Cd mixed ferrites," AIP Conf. Proc., vol. 2162, no. 1, p. 020083, Oct. 2019, doi: 10.1063/1.5130293.

[51] M. E. Mahmoud, M. F. Amira, S. M. Seleim, and A. K. Mohamed, "Adsorption Isotherm Models, Kinetics Study, and Thermodynamic Parameters of Ni(II) and Zn(II) Removal from Water Using the LbL Technique," J. Chem. Eng. Data, vol. 62, no. 2, pp. 839–850, Feb. 2017, doi: 10.1021/ACS.JCED.6B00865/ASSET/IMAGES/MEDIUM/JE-2016-00865W_0010.GIF.

[52] H. Darmokoesoemo, E. Prasetyo Kuncoro, G. Supriyanto, Y. Sri, and W. Manuhara, "Models, kinetics, and thermodynamics for the adsorption of Pb2+ and Cd2+ metal ions by solid tofu waste immobilized on silica's SURFAC," Moroccan J. Chem., vol. 8, no. 1, pp. 8-1 (2020) 012-023, Jan. 2020, doi: 10.48317/IMIST.PRSM/MORJCHEM-V8I1.19119.

[53] Z. Zhang and T. J. Pinnavaia, "Mesostructured γ-Al2O3 with a lathlike framework morphology," J. Am. Chem. Soc., vol. 124, no. 41, pp. 12294–12301, Oct. 2002, doi: 10.1021/JA0208299/ASSET/IMAGES/MEDIUM/JA0208299N00001.GIF.

[54] A. U. Haq, M. Saeed, M. Usman, M. Yameen, M. Muneer, and S. Tubbsum, "A comparative sorption study of Cr 3+ and Cr 6+ using mango peels: Kinetic, equilibrium and thermodynamic," Green Process. Synth., vol. 8, no. 1, pp. 337–347, Jan. 2019, doi: 10.1515/GPS-2019-0001/ASSET/GRAPHIC/J_GPS-2019-0001_FIG_010.JPG.

[55] X. H. Vu et al., "Adsorption of chromium(VI) onto freshwater snail shell-derived biosorbent from aqueous solutions: Equilibrium, kinetics, and thermodynamics," J. Chem., vol. 2019, no. Iii, 2019, doi: 10.1155/2019/3038103.

[56] S. Tamjidi and H. Esmaeili, "Chemically Modified CaO/Fe 3 O 4 Nanocomposite by Sodium Dodecyl Sulfate for Cr(III) Removal from Water," Chem. Eng. Technol., vol. 42, no. 3, pp. 607–616, Mar. 2019, doi: 10.1002/CEAT.201800488.

[57] J. Wang, R. Cao, D. He, and A. Saleem, "Facile preparation of polyethyleneimine modified activated sludge-based adsorbent for hexavalent chromium removal from aqueous solution," Sep. Sci. Technol., vol. 56, no. 3, pp. 498–506, 2021, doi: 10.1080/01496395.2020.1728324.

[58] F. Ahmadi and H. Esmaeili, "Chemically modified bentonite/Fe3O4 nanocomposite for Pb(II), Cd(II), and Ni(II) removal from synthetic wastewater," Desalin. Water Treat., vol. 110, no. May, pp. 154–167, 2018, doi: 10.5004/dwt.2018.22228.